Electron transport in high-resistance semiconductor nanowires through two-probe measurements

Yen-Fu Lin,[a] Tzu-Han Chen,[a] Chia-Hung Chang,[a] Yu-Wei Chang,[a] Yi-Cheng Chiu,[a] Hsiang-Chih Hung,[a] Ji-Jung Kai,[b] Zhaoping Liu,†[c] Jiye Fang[c] and Wen-Bin Jian*[a]

Received 26th March 2010, Accepted 24th May 2010
DOI: 10.1039/c0cp00038h

Since the successful fabrication of semiconductor nanowires, various techniques have been developed to contact these nanowires and to probe their intrinsic electrical properties. Although many novel quasi one-dimensional materials such as $Pb_{1-x}Mn_xSe$ nanoarrays were recently produced, their intrinsic electron transport properties have not been extensively studied so far. In this work, we demonstrate that an ordinary source–drain configuration of field-effect transistors or the two-probe measurement can be applied to the exploration of the intrinsic properties of nanowires. This two-probe measurement approach also works on highly resistive nanowires without an Ohmic contact issue. By using this method, electron transport behavior, resistivity, and carrier concentrations of ZnO, InP, GaP, and $Pb_{1-x}Mn_xSe$ semiconductor nanowires have been investigated. Due to the tiny cross-section and few conducting channels, a nanomaterial usually reveals an ultra high resistance. This technique demonstrates a two-probe characterization of nanostructures, paving the simplest way toward electrical characterizations of all high-resistance nanomaterials such as deoxyribonucleic acid (DNA), molecules and organics.

1 Introduction

Various semiconductor nanowires (NWs) have been synthesized by using either physical or chemical growth methods in the past decades. These NWs have been applied to single electron devices, field-effect transistors, optoelectronics, and nano-electronics through top-down or bottom-up approaches.[1] It is generally accepted that the conductivity of semiconductors results from an impurity-doping and native defects, such as vacancies, interstitials, and nonstoichiometry between two composing elements. NWs of a semiconductor could therefore exhibit a diverse electrical behavior individually. Additionally, semiconductor NWs have been used in demonstrations of novel functional electronic devices. Because most electronic devices have a two-probe configuration on the source and drain electrodes, identification and determination of intrinsic electrical properties of a NW through a systematic procedure of this two-probe approach should be vital for a real control and manipulation of NW-based electronics. This non-destructive testing technique is important for on-chip characterizations as well. Although four-probe techniques can accurately be used to exclude the contact resistance and to obtain intrinsic NW resistance under the condition of four Ohmic contacts, two-probe techniques are particularly useful for very short nanostructures. The two-probe technique is, nevertheless, inevitable for electrical characterizations of nanostructures.

ZnO is a II–VI semiconductor and reveals a variety of shapes and nanophase structures. It also demonstrates unusual characteristics in terms of doping modulated electrical conductivity, exciton and lasing demeanors, gas and optical sensing capabilities, and diluted-magnetic properties with dopants of magnetic impurities.[2] The first ZnO NW device exhibits a capacity for use as ultraviolet photodetectors and optical switches.[3] Since the time when ZnO NWs with dozens of micrometre in length were successfully synthesized and high doping to such NWs was available (in order to decrease the depletion length), several groups have presented a back gate effect on ZnO NW field-effect transistors at various temperatures.[4–8] In addition to the logic circuit operations of these NW devices, a temperature-dependent resistance, which uncovers intrinsic electron transport properties in the NWs, was also explored by two-[9,10] and four-probe[11] measurement techniques. These experimental results reveal thermally activated transport, Efros–Shklovskii variable range hopping, or three-dimensional Mott variable range hopping (VRH) in ZnO NWs.

Unlike the burgeoning output of experimental reports on ZnO NWs, the III–V semiconductors, InP and GaP NWs, have not been broadly studied. The most exciting phenomenon from n- and p-type doped InP NW devices prepared by laser-assisted catalytic growth[12] was a light-emitting diode on the nanoscale. Later on, InP NWs were also exercised as a spacer and barrier in InAs NWs for observation of a single-electron tunneling effect.[13] With the success of catalyst-free and self-seeded growth in solution, studies of current–voltage behavior

[a] *Department of Electrophysics, National Chiao Tung University, Hsinchu 30010, Taiwan. E-mail: wbjian@mail.nctu.edu.tw*
[b] *Department of Engineering and System Science, National Tsing Hua University, Hsinchu 30013, Taiwan*
[c] *Department of Chemistry, State University of New York at Binghamton, Binghamton, New York 13902-6000, USA*
† Current address: Ningbo Institute of Material Technology and Engineering, Chinese Academy of Sciences, Ningbo, Zhejiang, 315201, People's Republic of China

and fabrication of field-effect transistors on InP NW have just begun recently.[14–16] On the other hand, there are few reports on electrical properties of GaP NWs, possibly because of the difficulty in preparation and evaluation of NWs with such high resistivity. Moreover, although electrical properties of quantum dot arrays have been studied recently, the quantum dot assembled NWs, like our $Pb_{1-x}Mn_xSe$ semiconductor NWs,[17] have not been investigated deeply.

In this article, we present a practical strategy to determine the temperature-dependent resistance and to investigate the intrinsic electrical properties of ZnO, InP, GaP, and $Pb_{1-x}Mn_xSe$ NWs using a two-probe measurement technique. Because different syntheses might result in diverse concentrations of native defects, the resistivity of NWs could be altered from one sample to another.[18] Since the NWs for device fabrication in this work were deliberately picked from the same batch of samples, we assume that the resistivity of NWs from single as-synthesized samples should be in the same order of magnitude. On the other hand, the contact resistance could contribute enormously to the total resistance of the two-probe system, owing to the small nanocontact area.[19] We have made our best efforts in facilitating the Ohmic-contacted, NW-dominated devices so that the contact resistance can be neglected. In addition, by using a four-probe measurement system, we have confirmed the two-probe measurement of electron transport in ZnO NWs.

2. Experimental

ZnO NWs were synthesized by thermal evaporation (vapor transport) on quartz substrates with gold nanoparticles as catalysts to control the NW diameter.[20] InP and GaP NWs were synthesized by self-seeded, solution–liquid–solid growth[15] and they were stored in a toluene solvent. $Pb_{1-x}Mn_xSe$ ($0.002 \leqq x \leqq 0.008$) NWs (one-dimensional corrugated nanoarrays of $Pb_{1-x}Mn_xSe$ nanocrystals) were *in situ* self-assembled[17] and stored in a toluene solvent. NWs were analyzed by using a field-emission scanning electron microscope (FE-SEM, JEOL JSM-7000F). ZnO NWs are ~40 nm in diameter and 5–10 μm in length, whereas InP and GaP NWs are 2–5 μm in length and ~20 and ~30 nm in diameter, respectively. $Pb_{1-x}Mn_xSe$ NWs, however, possess the shortest length of 0.5–1 μm with a diameter of ~80 nm. Prior to the electron-beam (e-beam) lithography process, micrometre-scale Ti/Au electrodes and current leads were photo-lithographically generated on a Si wafer, capped with a 400-nm thick SiO_2 layer, in order to prevent current leakages through the substrate. In each experiment, the stocked ZnO, InP, or GaP NWs were dispersed on a pre-patterned substrate. FE-SEM was employed to locate the NWs. A standard e-beam lithography technique was used to pattern Ti/Au current leads and to contact the NWs. The as-fabricated two-probe NW devices were annealed at 400 °C in a high vacuum for 1 min in order to improve the contact. Due to a short length of $Pb_{1-x}Mn_xSe$ NWs, the e-beam lithography technique was firstly used to fabricate two Ti/Au current leads and connect to the large pattern, forming a gap of 200–300 nm in width between them. NWs were then positioned into the gap by a dielectrophoresis technique.[21] All of the two-probe NW devices were placed in a cryostat (Variable Temperature Insert Cryostat, CRYO Industries of America Inc.) for temperature-dependent current–voltage (I–V) measurements. The resistance was evaluated around the zero bias voltage from I–V data by linear least-square fitting. The temperature range for electron transport measurements is between 90 and 300 K.

3. Results and discussion

Fig. 1(a) displays a schematic diagram of a two-probe ZnO NW measurement system and the inset is a typical SEM image of a ZnO NW device. The scheme demonstrates that the NW was buried under the leads (electrodes) and contacted with Ti metal, having a contact area of $\sim 1 \times 0.04$ μm^2. The separation distance between two probes is a constant of ~1 μm. The targeted NWs were selected from the same source sample. Since these NWs have the same diameter and length, they should exhibit the same resistance. Fig. 1(b) presents data collected from three two-probe devices in which the NWs were detached from the same source sample. It was observed that not only are the room-temperature resistances of the three devices, ZnO-1, ZnO-2, and ZnO-3, largely different (up to four orders of magnitudes), but their temperature behavior is also disparate. According to above-mentioned assumption, that is, NWs of the same sample source should have defect concentration and resistances in the same order of magnitude, we propose that the higher resistance from ZnO-1 and ZnO-2 devices could be due to the nanocontact. This conjecture has been confirmed by current–voltage measurements which exhibit a nonlinear, non-Ohmic behavior.[19] As reported previously,[19] the nanocontact can be treated as a disordered system and the electron transport in nanocontact follows a theory of Mott VRH[22]

$$R = R_0 \exp\left(\left(\frac{T_0}{T}\right)^{1/p}\right) \quad (1)$$

where R and T are resistance and temperature, T_0 is a constant, R_0 is a weak temperature-dependent constant, and p is the exponent parameter. The dashed lines give the best fits to data in Fig. 1(b) to derive the exponent p of 2 and 4 for ZnO-2 and ZnO-1 devices, respectively. The increase of room-temperature resistance as well as disorder in the nanocontact can raise the exponent parameter p from 2 to 4 and the nanocontact-constrained electron system from one- to three-dimensional Mott VRH.

On the other hand, if a device, such as ZnO-3, holds the lowest room-temperature resistance, it implies that the intrinsic electrical property of the NW and the temperature-dependent resistivity may follow a thermally activated transport equation

$$R = R_0 \exp\left(\frac{E_A}{2k_B T}\right) \quad (2)$$

where R_0 is a constant, k_B is the Boltzmann constant, and E_A is the activation energy. The solid line in Fig. 1(b) presents the

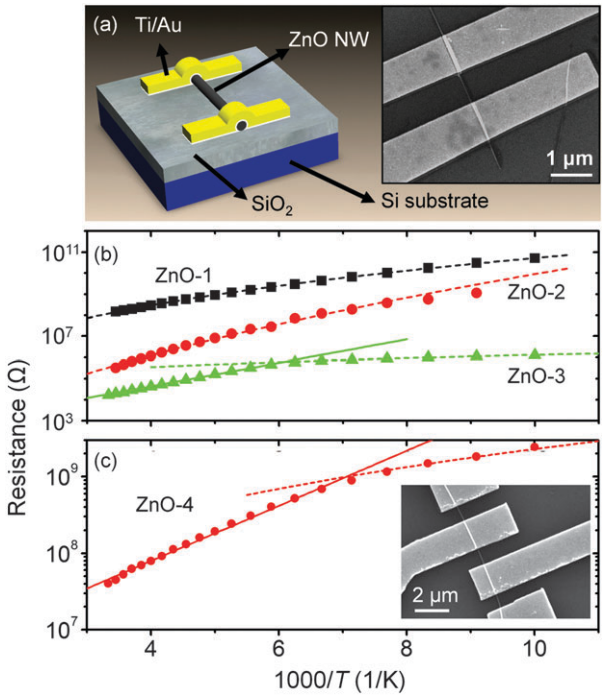

Fig. 1 (a) Schematic diagram of a two-probe ZnO NW device with a typical SEM image shown in the inset. Temperature-dependent resistance of (b) two- and (c) four-probe ZnO NW devices. A schematic diagram of a four-probe device is drawn in the inset of Fig. (c). Solid and dashed lines delineate the best fits to the mathematical forms of thermally activated transport and Mott VRH, respectively. After fitting to Mott VRH (dashed lines), the exponents, p's, of ZnO-1, ZnO-2, ZnO-3, and ZnO-4 devices are estimated to be 4, 2, 4, and 4, respectively.

best fit to the data of ZnO-3 device according to the thermally activated transport equation. The room-temperature resistance of ZnO-3 device is 16.8 kΩ and the length and diameter of the NW are 1 μm and 40 nm, respectively, resulting in a resistivity of ~0.002 Ω cm. Assuming that the electron mobility is 50 $cm^2\ V^{-1}\ s^{-1}$,[23] we can estimate the carrier concentration to be 10^{19} cm^{-3} at room temperature. At temperatures lower than 140 K, it is amazing to see that the temperature-dependent resistance deviates from the theoretically predicted values. Since a random distribution of native defects and a disorder are introduced, the electron transport in ZnO NWs, having a low carrier concentration, should follow Mott VRH at very low temperatures. The resistance of ZnO-3 device agrees well with the three-dimensional Mott VRH theory (the dashed line, $p = 4$) at temperatures lower than 140 K. To verify this conjecture, we adopted a four-probe measurement method (see Fig. 1(c)) and confirmed that the intrinsic NW transport follows the three-dimensional Mott VRH theory described in eqn (1) with the exponent parameter $p = 4$. This result is in consistent with a determination reported recently.[10] As a consequence, the two-probe measurement with two Ohmic contacts and low resistance can be employed in acquiring carrier concentration and electron transport properties in ZnO NWs. Furthermore, the source sample of ZnO-4 is different from that of ZnO-3 and the room-temperature resistivity and carrier concentration of ZnO-4 were evaluated to be 17 Ω cm and 10^{16} cm^{-3}, respectively. The carrier concentration of ZnO-4 NW is about three orders of magnitude lower than that of ZnO-3 NW. It should be pointed out that the ZnO NWs picked up from different source samples can exhibit extraordinarily discrepant resistivities and carrier concentrations, even though they are synthesized by the same growth method. The change in carrier concentrations among NWs picked up from different source samples is expected to come from varied concentrations of structure defects such as oxygen vacancies and Zn interstitials.

To extend the application of this two-probe measurement method to other semiconductor NWs, InP NW devices were fabricated through a solution-based growth[15] and a typical SEM image is presented in the inset of Fig. 2. InP NWs, like ZnO NWs, are natively n-type doped with a relatively low carrier concentration, which have been proved by the back gate effect (not shown in this report). Fig. 2 illustrates temperature-dependent resistances of InP-1, InP-2, and InP-3 devices. The InP NWs were picked up from the same source but their room-temperature resistances, 1100, 420, and 30 MΩ for InP-1, InP-2, and InP-3 devices, varied considerably. Like ZnO-1 and ZnO-2 devices, the high resistance of InP-1 and InP-2 might result from the nanocontact. The temperature behavior at higher temperatures can be fitted by the thermally activated transport theory (eqn (2), solid lines in Fig. 2), whereas those at temperatures lower than 150 K follow the Mott VRH theory (eqn (1), dashed lines). The exponent parameter p's are 2.4 and 4 for InP-2 and InP-1 devices, respectively, after fitting to Mott VRH in a low temperature range. It is noted that the Mott VRH theory can be solely used in fitting the data of the ZnO-1 device in the whole range of temperatures, whereas both the Mott VRH and thermally activated transport theories must be employed in fitting the data of InP-1 device. The difference comes from the NW resistance (resistivity). If the resistance (resistivity) of a NW is much lower, such as that of ZnO-3, the nanocontact resistance should dominate. Else, if they are comparable, the device characteristics will depend on contributions from both the NW and the nanocontact. Moreover, when thermally activated transport was used in fitting the data of InP NWs (InP-1, InP-2, and InP-3 devices) at high temperatures, the same slope of temperature-dependent resistance indicates the same activation energy (E_A) for carriers in InP NWs. On the other hand, since the InP-3 device holds the lowest resistance, it implies an intrinsic electron transport in the InP NW. In the case of InP-3, the NW was ~1 μm in length and ~20 nm in diameter and the resistivity was determined as ~0.94 Ω cm. Assuming that the electron mobility is 1000 $cm^2\ V^{-1}\ s^{-1}$,[24] the carrier concentration at room temperature can be estimated as $\sim 6.6 \times 10^{15}$ cm^{-3}. The temperature-dependent resistance of InP-3 device indicates that electron transport at high temperatures can be well described by the thermally activated transport theory, and at low temperatures it follows the three-dimensional Mott VRH theory ($p = 4$). It should be emphasized that, in nanocontact-dominated devices such as InP-1 and InP-2, the exponent parameter p of Mott VRH rises from 2.4 to 4 with an increasing room-temperature resistance of these InP NW devices. In contrast, in NW-dominated devices such as InP-3, the exponent parameter p of Mott VRH

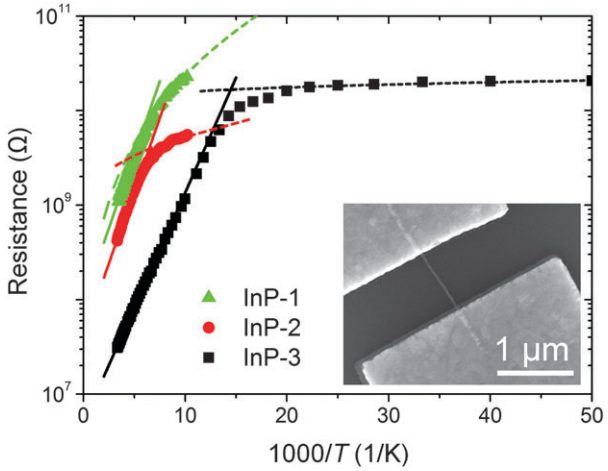

Fig. 2 (a) Resistance as a function of inverse temperature for two-probe InP NW devices with a typical SEM image shown in the inset. The solid and dashed lines delineate the best fits to mathematical equations of thermally activated transport and Mott VRH, respectively. After fitting to Mott VRH (dashed lines), the exponents, p's, for InP-1, InP-2, and InP-3 are estimated to be 4, 2.4, and 4, respectively.

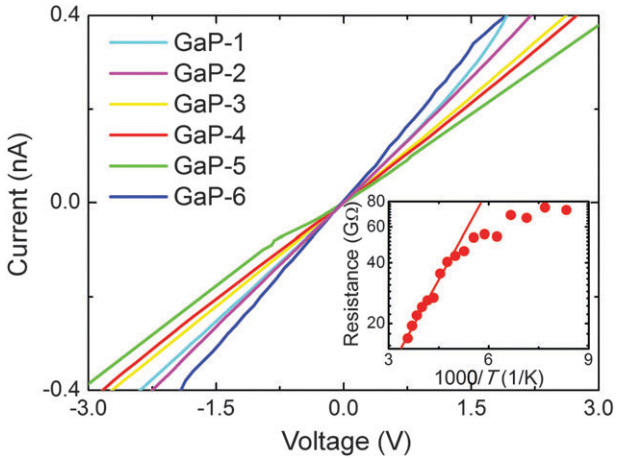

Fig. 3 I–V curves, taken at room temperature, from six different GaP NW devices. The inset shows temperature-dependent resistance of GaP-5 device. The solid line in the inset demonstrates the best fit to the thermally activated transport equation.

remains as a constant of ~4, implying three-dimensional Mott VRH in InP NWs.

As mentioned above, it was observed that, as the NW resistance (resistivity) increases, the resistance of a two-probe NW device will be dominated by the intrinsic NW resistance even though the contact is non-Ohmic and poor. We conclude, therefore, that the higher the NW resistance is, the easier the intrinsic electrical property of the NW can be drawn out. As for a contact area of $\sim 1 \times 0.04\ \mu m^2$, the contact resistance is typically no bigger than ~1 GΩ. Thus, NWs of room-temperature resistance no less than 1 GΩ could easily be determined by using the two-probe technique. This idea has been materialized in GaP NWs. I–V curves of all GaP devices are displayed in Fig. 3. The inset is the temperature-dependent resistance of GaP-5. It is worth noting that the I–V curves of all devices are linear over a wide range of voltage (from −3 to 3 V). This behavior can be observed in devices of high-resistance nanostructures such as NWs and nanocrystals. If electron transport in GaP NW follows the thermally activated transport theory, the I–V should reveal an Ohmic characteristic of this NW rather than of hopping conduction in a disordered system of the nanocontacts. As expected, the temperature-dependent resistance, shown in the inset of Fig. 3, implies thermally activated transport. For example, GaP-5 which are 1 μm and 20 nm in length and diameter, respectively, exhibit a room-temperature resistance of 8.1 GΩ and a resistivity of ~254 Ω cm. Assuming that the electron mobility is 160 $cm^2\ V^{-1}\ s^{-1}$,[25] we can therefore estimate the carrier concentration as $1.53 \times 10^{14}\ cm^{-3}$ at room temperature.

Since $Pb_{1-x}Mn_xSe$ NWs are too short to be connected with submicron electrodes by e-beam lithography, a dielectrophoresis technique[21] was alternatively applied to the assembly of two-probe devices. Fig. 4(a) is a scheme of the short-NW device. The morphology and dimensions of $Pb_{1-x}Mn_xSe$ NWs (or nanoarrays) were determined using SEM image and shown in the inset of Fig. 4(a). It is conventionally proposed that the transport may be dominated by electron tunneling among $Pb_{1-x}Mn_xSe$ nanocrystals in this particularly corrugated NW. In addition, the intrinsic transport through electron tunneling might give a high resistance so as to neglect the contact effects. As shown in the inset of Fig. 4(b), the SEM image indicates that a few $Pb_{1-x}Mn_xSe$ NWs sit on the two probes in the PbMnSe-1 device. Its electron transport (Fig. 4(b)) shows extremely high and temperature-independent resistance in a temperature range between 100 and 300 K. The temperature-independent behavior implies that a tunneling barrier must be much higher than the thermal energy at room temperature. On the other hand, a dielectrophoresis can be utilized to position a large amount of NWs on two probes. As shown by a SEM image presented in the inset of Fig. 4(c), for example, the PbMnSe-2 device containing dozens of $Pb_{1-x}Mn_xSe$ NWs shows a strong temperature-dependence resistance. In Fig. 4(c), the solid line indicates the best fit, according to the fluctuation-induced tunneling theory of the form[26]

$$R = R_0 \exp\left(\frac{T_1}{T_0 + T}\right) \qquad (3)$$

where T_0 and T_1 are constants. The temperature behavior of PbMnSe-2 complies thoroughly with the fluctuation-induced tunneling theory. The agreement not only supports our assumption of tunneling-dominated electron transport among $Pb_{1-x}Mn_xSe$ nanocrystals in the corrugated NWs, but also confirms the temperature-independent tunneling resistance observed from PbMnSe-1 over the whole range of temperatures. Moreover, the low-temperature resistance (< 100 K) of PbMnSe-1 is about several dozen-fold higher than that of PbMnSe-2 due to the fact that the number of NWs in PbMnSe-1 is several dozen-fold less than that in PbMnSe-2. The result indicates that the low-temperature resistance of the device is the total resistance of $Pb_{1-x}Mn_xSe$ NWs connected in parallel.

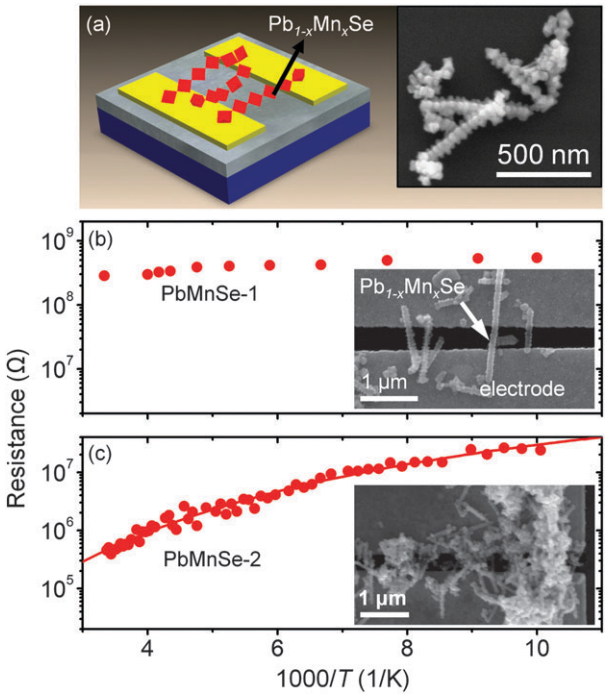

Fig. 4 (a) Schematic diagram of a two-probe $Pb_{1-x}Mn_xSe$ NW device. The SEM image of $Pb_{1-x}Mn_xSe$ NWs is shown in the inset. Temperature-dependent resistance of (b) PbMnSe-1 and (c) PnMnSe-2 devices with their SEM images are presented in the insets. The solid line indicates the best fit to the theory of fluctuation-induced tunneling conduction.

4. Conclusion

In summary, a two-probe technique used in determining intrinsic electrical properties of NWs was demonstrated. In the case that a nancontact resistance is superior or comparable to a NW resistance, low resistance at room temperature implies an electron transport nature in NWs. In contrast, effects of the nanocontact can be neglected if the NW resistance is considerably high. Using this two-probe technique, we determined that electron transport in ZnO and InP NWs at high temperatures is thermally activated transport and it follows three-dimensional Mott VRH at low temperatures. The study further shows that electron transport in GaP NWs is thermally activated transport. Based on this two-probe measurement, room-temperature carrier concentrations of our as-synthesized ZnO, InP, and GaP NWs have been evaluated to be 10^{19} (for ZnO-3 NW), 6.6×10^{15}, and 1.53×10^{14} cm^{-3}, respectively. These results also indicate that the ZnO NWs picked up from different source samples give discrepant resistivities and carrier concentrations at room temperature. Moreover, electron transport in $Pb_{1-x}Mn_xSe$ NWs exhibits temperature-independent tunneling resistance in a temperature range between 100 and 300 K, whereas electron transport in entangled $Pb_{1-x}Mn_xSe$ NWs presents a fluctuation-induced tunneling transport. Using this two-probe approach, electron transport properties in ZnO, InP, GaP, and $Pb_{1-x}Mn_xSe$ NWs have been systematically evaluated and discussed.

Acknowledgements

This work was supported by the Taiwan National Science Council under Grant Numbers NSC 98-2112-M-009-013-MY2 and NSC 98-2923-M-009-001-MY2, and by the MOE ATU Program. JF thanks US NSF support (DMR-0731382).

References

1 W. Lu and C. M. Lieber, *Nat. Mater.*, 2007, **6**, 841.
2 C. Klingshirn, *ChemPhysChem*, 2007, **8**, 782.
3 H. Kind, H. Yan, B. Messer, M. Law and P. Yang, *Adv. Mater.*, 2002, **14**, 158.
4 Y. W. Heo, L. C. Tien, Y. Kwon, D. P. Norton, B. S. Pearton, B. S. Kang and F. Ren, *Appl. Phys. Lett.*, 2004, **85**, 2274.
5 W. I. Park, J. S. Kim, G. C. Yi, M. H. Bae and H. J. Lee, *Appl. Phys. Lett.*, 2004, **85**, 5052.
6 Z. Fan, D. Wang, P. C. Chang, W. Y. Tseng and J. G. Lu, *Appl. Phys. Lett.*, 2004, **85**, 5923.
7 Q. H. Li, Y. X. Liang, Q. Wan and T. H. Wang, *Appl. Phys. Lett.*, 2004, **85**, 6389.
8 J. Goldberger, D. J. Sirbuly, M. Law and P. Yang, *J. Phys. Chem. B*, 2005, **109**, 9.
9 Y. J. Ma, Z. Zhang, F. Zhou, L. Lu, A. Jin and C. Gu, *Nanotechnology*, 2005, **16**, 746.
10 P. C. Chang and J. G. Lu, *Appl. Phys. Lett.*, 2008, **92**, 212113.
11 S. P. Chiu, Y. H. Lin and J. J. Lin, *Nanotechnology*, 2009, **20**, 015203.
12 X. Duan, Y. Huang, Y. Cui, J. Wang and C. M. Lieber, *Nature*, 2001, **409**, 66.
13 C. Thelander, H. A. Nilsson, L. E. Jensen and L. Samuelson, *Nano Lett.*, 2005, **5**, 635.
14 N. P. Kobayashi, V. J. Logeeswaran, M. S. Islam, X. Li, J. Straznicky, S. Y. Wang, R. S. Williams and Y. Chen, *Appl. Phys. Lett.*, 2007, **91**, 113116.
15 Z. Liu, K. Sun, W. B. Jian, D. Xu, Y. F. Lin and J. Fang, *Chem.–Eur. J.*, 2009, **15**, 4546.
16 T. Strupeit, C. Klinke, A. Kornowski and H. Weller, *ACS Nano*, 2009, **3**, 668.
17 W. Lu, P. Gao, W. B. Jian and Z. L. Wang, *J. Am. Chem. Soc.*, 2004, **126**, 14816.
18 E. Schlenker, A. Bakin, T. Weimann, P. Hinze, D. H. Weber, A. Gölzhäuser, H. Wehmann and A. Waag, *Nanotechnology*, 2008, **19**, 365707.
19 Y. F. Lin and W. B. Jian, *Nano Lett.*, 2008, **8**, 3146.
20 W. B. Jian, I. J. Chen, T. C. Liao, Y. C. Ou, C. H. Nien, Z. Y. Wu, F. R. Chen, J. J. Kai and J. J. Lin, *J. Nanosci. Nanotechnol.*, 2008, **8**, 202.
21 H. A. Pohl, *Dielectrophoresis*, Cambridge University, London, 1978.
22 N. F. Mott, *Conduction in Non-Crystalline Materials*, Clarendon Press, Oxford, 1993 p 32.
23 P. C. Chang, C. J. Chien, D. Stichtenoth, C. Ronning and J. G. Lu, *Appl. Phys. Lett.*, 2007, **90**, 113101.
24 E. D. Minot, F. Kelkensberg, M. van Kouwen, J. A. van Dam, L. P. Kouwenhoven, V. Zwiller, M. T. Borgstro1m, O. Wunnicke, M. A. Verheijen and E. P. A. M. Bakkers, *Nano Lett.*, 2007, **7**, 367.
25 J. R. Kim, B. K. Kim, J. O. Lee, J. Kim, H. J. Seo, C. J. Lee and J. J. Kim, *Nanotechnology*, 2004, **15**, 1387.
26 P. Sheng, K. Sichel and J. L. Gittleman, *Phys. Rev. Lett.*, 1978, **40**, 1197.

